Vibrations of porphycene in the S−0 and S−1 electronic states: Single vibronic level dispersed fluorescence study in a supersonic jet

ARTICLE *in* THE JOURNAL OF CHEMICAL PHYSICS · MAY 2013

Impact Factor: 2.95 · DOI: 10.1063/1.4802769 · Source: PubMed

4 AUTHORS:

Ephriem Mengesha
Atomic Energy and Alternative Energies Com…
3 PUBLICATIONS **4** CITATIONS
SEE PROFILE

Jerzy Sepioł
Instytut Chemii Fizycznej PAN
56 PUBLICATIONS **922** CITATIONS
SEE PROFILE

Paweł Borowicz
Institute of Electron Technology
54 PUBLICATIONS **617** CITATIONS
SEE PROFILE

J. Waluk
Polish Academy of Sciences
256 PUBLICATIONS **3,670** CITATIONS
SEE PROFILE

Vibrations of porphycene in the S_0 and S_1 electronic states: Single vibronic level dispersed fluorescence study in a supersonic jet

Ephriem T. Mengesha, Jerzy Sepioł, Paweł Borowicz, and Jacek Waluk
Institute of Physical Chemistry, Polish Academy of Sciences, Kasprzaka 44, 01-224 Warsaw, Poland

(Received 26 February 2013; accepted 9 April 2013; published online 1 May 2013)

Supersonic jet-isolated porphycene has been studied using the techniques of laser-induced fluorescence excitation, single vibronic level fluorescence, and spectral hole burning, combined with quantum mechanical calculations of geometry and vibrational structure of the ground and lowest electronically excited singlet states. Porphycene is a model for coherent double hydrogen tunneling in a symmetrical double well potential, as evidenced by tunneling splittings observed in electronic absorption and emission. The results led to reliable assignment of low frequency modes in S_0 and S_1 electronic states. The values of tunneling splitting were determined for ground state vibrational levels. In the case of tautomerization-promoting $2A_g$ mode, tunneling splitting values significantly increase with the vibrational quantum number. Mode coupling was demonstrated by different values of tunneling splitting obtained for coexcitation of two or more vibrations. Finally, alternation of relative intensity patterns for the components of $2A_g$ tunneling doublet observed for excitation and emission into different vibrational levels suggests that the energy order of levels corresponding to (+) and (−) combinations of nuclear wave functions is different for even and odd vibrational quantum numbers. © *2013 AIP Publishing LLC*. [http://dx.doi.org/10.1063/1.4802769]

I. INTRODUCTION

Since the synthesis of porphycene[1] (Scheme 1(a)) as the first constitutional isomer of porphyrin (Scheme 1(b)), numerous studies have been devoted to photophysical characterization and potential applications of this compound and its derivatives.[2–7] Although porphycene retains the central feature of porphyrin, a cavity with four nitrogen atoms and two inner exchangeable hydrogen atoms, it differs from porphyrin in the cavity shape, NH···N distances, overall symmetry, and in the intensity pattern of electronic absorption. The lowest electronic transition (Q_1 band) in porphycene is more than an order of magnitude stronger than that of porphyrin and also significantly redshifted. This feature, along with other photophysical characteristics, makes porphycene a potentially much better agent for photodynamic therapy than parent porphyrin and its derivatives.[3,4,8–12] Differences between porphyrin and porphycene have also been observed in the rates and mechanism of intramolecular tautomerization. NMR study of crystalline porphycene[13] showed the presence of four different tautomers of which the interconversion turned out to be very fast on the NMR time scale even at 107 K. On the other hand, the interconversion between two equivalent *trans* tautomers of porphyrin in the ground state is strongly temperature-dependent. The reported rate at 298 K is 2×10^4 s^{-1}, whereas below 230 K the tautomerization stops.[14] Owing to its rigid geometry, isolated cavity, and small NH···N distances, porphycene provides a good model system for studying intramolecular hydrogen transfer dynamics, especially when the investigation is undertaken in a supersonic jet, where the study of cold isolated molecules is possible.

The first supersonic jet study of porphycene was reported by Sepioł *et al.*,[15] who demonstrated that the 0-0 and all the vibronic bands observed in the laser-induced fluorescence (LIF) excitation spectrum were split into doublets. The doublets disappear upon exchange of one or both protons in the cavity by deuterons, as well as upon complexation with water or alcohol. This observation was interpreted as evidence of coherent double hydrogen tunneling in a symmetric double minimum potential. The fact that all the vibronic doublet lines are equally spaced, along with the temperature dependence of LIF excitation spectra of porphycene, showed that the ground state tunneling splitting is larger than the excited state splitting, suggesting a higher energy barrier or larger barrier width in the excited state than in the ground electronic state. This suggestion was confirmed by the results of studies of tautomerization in condensed phases.[16–22] A methodology was developed, based on polarized spectroscopy techniques, both in emission and transient absorption, which enabled to determine the tautomerization rates in S_0 and S_1 for the parent porphycene and several derivatives. The reaction rates in the lowest excited singlet state are several times lower than in S_0. Moreover, the values of the rates vary for differently substituted porphycenes by several orders of magnitude (10^9-10^{13} s^{-1}); the isotope effects, measured at 293 K, are also substantial.[19] These findings indicate the importance of tunneling even at room temperature.

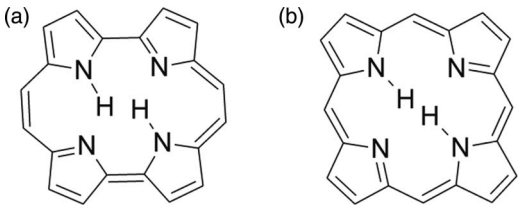

SCHEME 1. Structural formulas of porphycene (a) and porphyrin (b).

In another investigation, Vdovin *et al.*[23] reported supersonic jet studies of porphycene and 9,10,19,20-alkylated porphycenes. It was shown that the tunneling splitting is affected by alkyl substitution, which leads to a decrease of the NH · · · N distance in the cavity, one of the key parameters in hydrogen transfer dynamics. Applying a simple 1D model, they have estimated a hydrogen transfer barrier height of 217-1360 cm^{-1} using the experimental value of the ground state tunneling, 4.4 cm^{-1}, and varying the tunneling mass m between 1 and 2 and the tunneling distance between 0.55 and 0.65 Å. These values yielded an impinging frequency ν ranging between 185 and 673 cm^{-1}. However, for the alkylated derivatives the results of this work actually demonstrated that the 1D model cannot account for the intensity pattern of the observed spectral features. These features could be explained by assuming an asymmetric double well potential along the tautomerization coordinate, both for *trans-trans* and *cis-cis* interconversions. The origin of the asymmetry is the coupling between the movement of the inner hydrogens and the torsional modes of alkyl substituents. Interestingly, the asymmetry becomes reversed upon passing from S_0 to S_1.

High resolution optical spectroscopic study of porphycene doped in superfluid helium nanodroplets[24] showed tunneling splittings of 4.4 and 0.58 cm^{-1} for porphycene and monodeuterated porphycene (Pc-d_1), respectively, from LIF excitation spectral measurement. Dispersed fluorescence spectral measurement via excitation of the origin band revealed the doublets for various vibrational modes, differing in the magnitude of the splitting and intensity distribution. The observed differences reflect different tunneling probabilities for the respective vibrational modes in the S_0 state. This picture was confirmed by theoretical studies,[25] based on Car-Parinello molecular dynamics simulations.

The above results show clearly that, in order to properly describe the tautomerization path in porphycenes, absolutely crucial is the knowledge of vibrational structure in the S_0 and S_1 electronic states. Initial studies brought a surprising result: the experimental IR spectra lacked the presence of the NH stretching band, predicted by harmonic calculations to be the strongest in the spectrum.[26] This behavior was explained in a recent work,[27] which combined IR, Raman, fluorescence, and inelastic neutron scattering (INS) with *ab initio* molecular dynamics simulations. Coupling of the NH stretching with other modes was shown to be responsible for the extreme broadening of the NH band, leading to difficulties in its detection.

The present work, along with our previous studies,[23,24,27] represents an effort towards a full and accurate characterization of the vibrational structure of porphycene. The precise assignment of vibrations both in S_0 and S_1 electronic states should help to understand the pattern of mode coupling (and hence dimensionality of hydrogen tunneling coordinate). This task is not trivial, not only due to the large number of vibrational mode in porphycene (108), but also because of the presence of tunneling splittings, different for different vibrations and electronic states. To overcome these difficulties, we focus on the analysis of LIF and single vibronic level dispersed fluorescence spectra of porphycene in supersonic jet. We exploit the fact that effective collisions, and hence random thermalizations, are highly prohibited in supersonic jet, and therefore the technique allows to see fluorescence occurring from unrelaxed vibronic levels in the S_1 state, which can be used for precise assignments of vibrations, observation of mode-selective tunneling splittings, and the study of mode coupling.

II. EXPERIMENTAL AND COMPUTATIONAL DETAILS

The synthesis and purification of porphycene has been described in Ref. 1. The experimental setup was described in detail in Ref. 23. Three types of spectra: LIF excitation, hole burning, and dispersed fluorescence, have been recorded. Porphycene sample heated to 520 K was expanded with helium carrier (3 atm) to a vacuum chamber through a homemade pulsed valve based on IOTA Series 9, General Valve in a nozzle of about 500 μm diameter. The expanded sample beam was excited at 7 mm from the nozzle with a narrow band (<0.1 cm^{-1}) optical parametric oscillator (OPO, Sunlite Ex, Continuum) pumped by a seeded Nd:YAG laser (Powerlite 8000, repetition rate 10 Hz). LIF excitation spectrum was detected by a Hamamatsu R2949 photomultiplier using a BG 645 cutoff filter. The signal was measured using a four-channel digital oscilloscope (YOKOGAWA DL9140). For hole-burning measurements (also called two-color laser depletion), a homemade dye laser pumped by Nd:YAG laser (Surelite I-10, Continuum) was used as a pumping source, while the OPO served as a probe laser. The delay between pump and probe pulses was about 200 ns. In our procedure, the pump laser is fixed at a wavelength resonant with an electronic transition of a selected species while scanning with the probe laser. The measurement is done with the pump laser on and off using a shutter at each step of the scan, which results in two LIF excitation spectra (a so-called active baseline procedure). Because the fluorescence intensity is proportional to the number of ground state species, it decreases for the selected species after pumping. A lowering of the intensity of vibronic bands belonging to the selected species is observed, while the intensities of bands belonging to the other species are unaffected by the pumping process. Dispersed fluorescence spectra were measured using a 0.5 m monochromator (Sciencetech 9040) attached to a CCD (Andor iDUS) camera. All the presented spectra are background-corrected by subtracting a respective background signal measured when laser pulses pass the jet area before valve opening. In all experiments, sample contamination from carrier gas impurities was avoided by passing the gas tube through a bath of liquid nitrogen.

Geometry optimizations and frequency calculations were done at the density functional theory (DFT) level, using both double zeta (B3LYP/6-31G(d,p)) and triple zeta (B3LYP/6-311++G(d,p)) basis sets. Time-dependent DFT (TD-DFT) model was applied for the excited state calculations with the same functional and basis sets using GAUSSIAN 09 program package.

III. RESULTS AND DISCUSSION

A. LIF excitation and hole burning spectra

Although the LIF excitation spectra of porphycene seeded in supersonic jet have already been reported,[15,23,24]

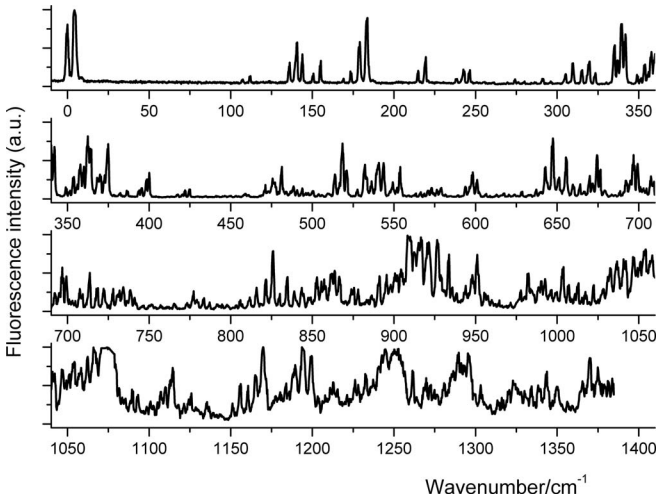

FIG. 1. LIF excitation spectrum of porphycene in the range up to 1400 cm^{-1} excess energy above the origin of the S_0-S_1 electronic transition.

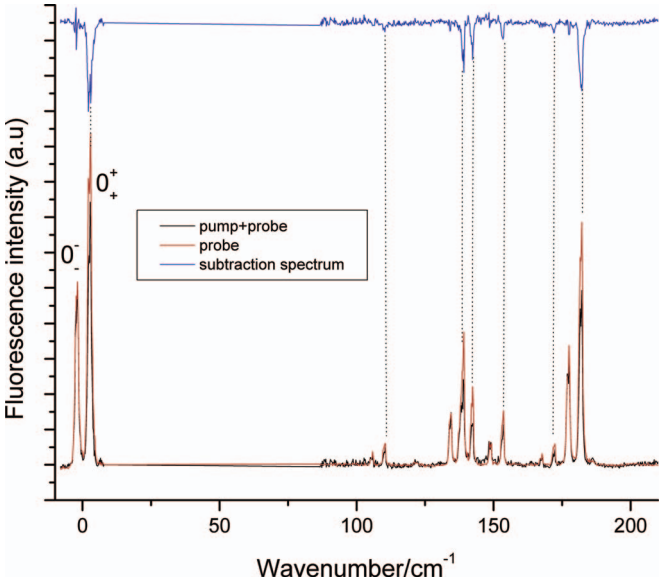

FIG. 2. Active baseline subtraction spectrum (top, blue) of porphycene obtained while pumping the 0^+_+ band of the LIF excitation spectrum. The scanning probe laser was delayed by 200 ns with respect to the fixed pump laser. (Bottom) The spectra obtained with and without pumping (black and red, respectively).

the measurement was repeated in an extended range up to 1400 cm^{-1} above the 0-0 transition (Figure 1). To achieve a much higher sensitivity, the LIF spectra were obtained in the saturation regime. Instead of typical pulses of 10-100 μJ energy, pulses of ~1 mJ were applied. This enabled observing many more transitions than detected before. For example, in addition to previously observed two transitions in the range below 200 cm^{-1} from the origin, four more transitions are identified, each composed of a doublet (Table I).

For the assignment of S_1 vibrations, it is helpful to note that the LIF spectrum consists of doublets, equally spaced for each vibrational mode by about 4.5 cm^{-1}. This behavior is a consequence of the fact that the tunneling splitting is practically negligible in S_1 (<0.2 cm^{-1}). Therefore, the constant spacing between the components of each doublet reflects the value of the ground state splitting in the vibrationally unexcited level. Moreover, the selection rules dictate that only the transitions between the states of equal parity of nuclear functions are allowed. Since the "plus" combination of wave functions lies below the "minus" one, the 0^-_- electronic transition of "hot" nature is located ~4.5 cm^{-1} below 0^+_+.[15] This pattern is repeated for the observed vibronic transitions. A vibrational mode frequency in S_1 therefore corresponds to the difference between the value observed for the lower energy component of each doublet and the value of 0^-_- transition that is the origin of the LIF spectrum.

The constant intensity pattern for the tunneling doublets is observed throughout the LIF spectra, the lower energy component always being weaker. Assuming the 4.5 cm^{-1} separation of the levels leads to an estimation of effective temperature of about 10 K.

Additional help in the vibrational assignments comes from hole-burning experiments, which allow differentiating between the transitions originating in the plus and minus ground state levels. An example is presented in Figure 2. The bands which respond to hole burning while pumping at the 0^+_+ band correspond to the transitions which originate in the "plus," lower energy level of S_0; those which originate from the "minus" population, do not respond.

The LIF excitation spectrum shows well-resolved vibronic bands up to about 800 cm^{-1}. The spectrum becomes broader for excitation above 800 cm^{-1}, indicating an onset of fast excited state dynamics (see below).

The use of saturation while recording the LIF spectra of porphycene resulted in the lack of simple one-to-one correspondence between the LIF excitation and origin-excited dispersed fluorescence spectra (Figure 3). The former reveals many more spectral features. For example, in the region below 180 cm^{-1}, only two bands appear in the dispersed fluorescence spectra at 152 and 145 cm^{-1}, whereas at least 5

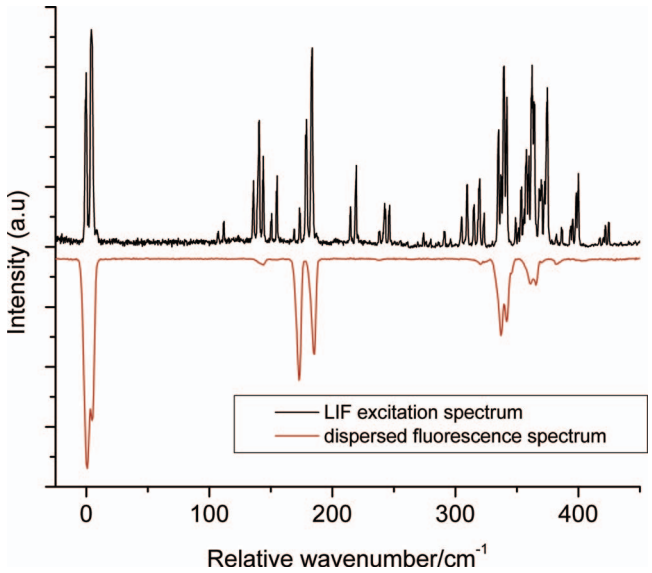

FIG. 3. Comparison of LIF excitation (black, top) and dispersed fluorescence (red, bottom) spectra of porphycene in supersonic jet. Fluorescence intensity in the dispersed fluorescence spectrum is multiplied by −1 for easier comparison.

TABLE I. Ground and excited state (S_1) vibrational frequencies of porphycene obtained from LIF and SVL fluorescence spectra.

$\tilde{\nu}$ (S_1)[a] expt.	$\tilde{\nu}$ (S_1)[b] calc	$\tilde{\nu}$ (S_0)[c] expt.	$\tilde{\nu}$ (S_0)[d] calc	$\Delta\tilde{\nu}$ (S_1-S_0) expt.	$\Delta\tilde{\nu}$ (S_1-S_0) calc	Assignment
107, 112	107	112, 116	117	−10	− 10	$1B_g$
		117, 121				
136, 141	129	135, 140	130	−4	− 1	$2B_g$
		140, 145				
139sh, 144	146	…	147	−4[e]	− 1	$1A_g$
		145				
150, 155	152	148, 152	154	−2	− 2	$2A_u + 3A_u$
		152, 156				
169, 174	174	162, 166	168	3	6	$2 \times 3A_u$
		166, 170				
179, 184	179	169, 181	185	1[e]	− 6	$2A_g$
		174, 186				
215, 220	214	235	234	−20	− 20	$2 \times 1B_g$
		239				
238, 242	237	260	260	−22	− 23	$1B_g + 2 \times 2A_u$
		…				
242, 246	236	260, 264	247	−22	− 11	$1B_g + 2B_g$
		263				
269, 274	258	…	260	…	− 2	$2 \times 2\ B_g$
276, 280	275	…	277	…	− 2	$1A_g + 2B_g$
287, 291	286	…	302	…	− 16	$2A_g + 1B_g$
293, 297	298	…	301	…	− 3	$1A_g + 2A_u + 3A_u$
305, 309	315	319	322	−14	− 7	$2B_g + 3B_g$
		324				
315, 320	308	310, 319	315	6	− 7	$2A_g + 2B_g$
		310, 318				
318, 323	325	…	332	−12	− 7	$1A_g + 2A_g$
		324, 336				
335, 339	340	335, 340	342	−5	− 2	$3A_g$
		337, 341				
337, 342	344	…	369	−24	− 25	$1A_u + 5A_u$
		361				
349, 354	346	…	364	−23	− 18	$2 \times 1B_g + 2B_g$
		371				
351, 356	360	…	381	…	− 21	$1A_g + 2 \times 1B_g$
358, 362	358	358	370	2[e]	− 12	$2 \times 2A_g$
		345, 364				
360, 364	367	357, 362	365	−2	2	$4A_g$
		361, 364				
369, 373	365	…	377	…	− 12	$1B_g + 2 \times 2B_g$
371, 375	366	…	387	−21	− 21	$1Bg + 2B_g + 2 \times 2A_u$
		392				
382, 387	382	…	394	…	− 12	$1A_g + 1B_g + 2B_g$
	388	…	402	…	− 14	$2 \times 1B_g + 2 \times 3A_u$
394, 398	394	408, 413	419	−19	− 25	$2A_g + 2 \times 1B_g$
		411, 418				
395, 400	355	399	390	−4	− 35	$5B_g$
		398				
417, 422	416	…	442	…	− 26	$2A_g + 1B_g + 2 \times 2A_u$
420, 425	415	…	432	…	− 17	$2A_g + 1B_g + 2B_g$
	410	…	424	…	− 4	$2 \times 2B_g + 2A_u + 3A_u$
471, 475	469	469, 474	472	−4	− 3	$3A_g + 2B_g$
		…				
476, 481	483	472, 476	482	−5	1	$5A_g$
		481				
484, 489	472	…	494	…	− 22	$2x(1B_g + 2B_g)$
491, 494	489	…	511	…	− 22	$1A_g + 2 \times 1B_g + 2B_g$
496, 500	496	…	495	…	1	$4A_g + 2B_g$
504, 509	494	…	507	…	− 13	$1B_g + 3\ x2B_g$

TABLE I. (*Continued*.)

$\tilde{\nu}$ (S_1)[a] expt.	$\tilde{\nu}$ (S_1)[b] calc	$\tilde{\nu}$ (S_0)[c] expt.	$\tilde{\nu}$ (S_0)[d] calc	$\Delta\tilde{\nu}$ (S_1-S_0) expt.	$\Delta\tilde{\nu}$ (S_1-S_0) calc	Assignment
514, 518	519	509, 522 514, 526	527	−4[e]	− 8	$2A_g + 3A_g$
516, 521	523	… 540, 555	554	−30[e]	− 31	$2A_g + 1A_u + 5A_u$
528, 532	522	… 548, 563	549	−26[e]	− 27	$2A_g + 2 \times 1B_g + 2B_g$
536, 541	537	… 542	555	−5	− 18	$3 \times 2A_g$
539sh, 544	546	… 536, 545	550	−7[e]	− 4	$2A_g + 4A_g$
547, 552	544	…	562	…	− 18	$2A_g + 1B_g + 2 \times 2B_g$
549, 554	554	…	576	…	− 22	$3A_g + 2 \times 1B_g$
594, 598	595	…	627	…	− 32	$2x\ 2A_g + 1B_g + 2 \times 2A_u$
596, 601	599	…	601	…	− 2	$6A_g$
643, 647	650	… 661	664	−18	− 14	$7A_g$
651, 656	650	…	664	…	− 14	$2A_g + 3A_g + 2B_g$
660, 664	651	…	679	…	− 28	$2A_g + 2x(1B_g + 2B_g)$
670, 674	668	…	696	…	− 28	$1A_{g+}\ 2A_g + 2 \times 1B_g + 2B_g$
672, 677	680	678 …	684	−6	− 4	$2 \times 3A_g$
692, 697	698	…	712	…	− 14	$2 \times 2A_g + 3A_g$
695, 699	707	…	707	…	0	$3A_g + 4A_g$
709, 714	701	…	734	…	− 32	$2 \times 2A_g + 2 \times 1B_g + 2B_g$
812, 816	823	…	824	…	− 1	$3A_g + 5A_g$
822, 826	829	… 851	849	−29	− 20	$2A_g + 7A_g$
830, 835	836	…	837	…	− 1	$3A_g + 4A_g + 2B_g$
839,844	830	…	864	…	− 34	$2x\ (2A_g + 1B_g + 2B_g)$

[a]Tunneling doublets observed in LIF, energy relative to the location of the 0_-^- transition.
[b]B3LYP/6-311++G(d,p), scaling factor 0.9960.
[c]Observed shifts with respect to the excitation into the lower (first row) and higher energy (second row) doublet component.
[d]B3LYP/6-311++G(d,p), scaling factor 0.9902.
[e]S_0 frequency value approximated taking into account different tunneling splittings in the vibrationless and vibrationally excited levels.

bands are observed in the vicinity of 140 cm^{-1} in the LIF excitation spectrum. An even larger difference is observed for the 200–300 cm^{-1} range. Therefore, the assignment of corresponding vibrations in the S_0 and S_1 states is not straightforward. The unambiguous assignment of each vibronic state becomes possible after recording the dispersed fluorescence spectra following excitation into different vibronic bands.

B. Single vibronic level dispersed fluorescence spectra

Dispersed fluorescence spectrum from a single vibronic level (SVL) provides information complementary to the excitation spectrum. It maps the overlap of the nuclear wave functions of the excited and ground electronic states and hence such measurements are essential for the precise assignment of vibrational levels both in the S_0 and S_1 states.[28–31] They also provide information about the extent of state mixing into the precursor of intramolecular vibrational energy redistribution (IVR). Single vibronic level fluorescence spectra originating from an excited vibrational level may provide detailed information on the ground state potential of analogous level. In this section, the dispersed fluorescence spectra of porphycene are presented and the bands are assigned with the aid of quantum chemical calculations.

1. 0_0^0 Excitation

The dispersed fluorescence spectrum of porphycene obtained via excitation of the high-energy component of the origin doublet (16 163 cm^{-1}) is presented in Figure 4. The spectrum exhibits features similar to those reported from earlier supersonic jet measurements,[23] but with better spectral resolution and sensitivity. Because of that, additional transitions could be detected. In the region up to 800 cm^{-1}, several previously unobserved small intensity bands have been identified. The assignments of the vibrations are presented in Table I.

Figure 5(a) presents a comparison of dispersed fluorescence spectra following 0_+^+ and 0_-^- excitations, respectively. The two spectra are very similar in the intensity distribution, as well as in the frequencies of the vibronic bands, except that, when plotted relative to the excitation energy, the vibronic pattern obtained for the 0_-^- excitation is shifted by 4-5 cm^{-1} towards lower values. This result is in line with the

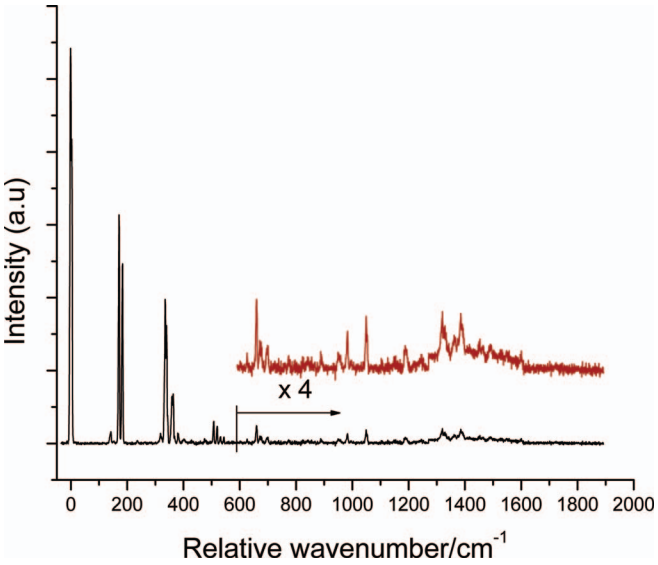

FIG. 4. Dispersed fluorescence spectrum of porphycene recorded for excitation into the 0^+_+ origin band (16 163 cm^{-1}). Frequencies are given in wavenumbers relative to the excitation energy.

assignment of the bands at 16 158 and 16 163 cm^{-1} as the tunneling components of the zero-point-energy level. Guided by the 4.4 cm^{-1} characteristic splitting and similarity of the corresponding fluorescence emission spectra, we are able to identify numerous pairs of tunneling doublets in the LIF spectrum of porphycene (Table I).

2. Excitation into low-energy vibronic bands

Figure 5 shows dispersed fluorescence spectra obtained for excitation into several representative tunneling doublets of porphycene. Similar spectroscopic features assigned to tunneling doublets have also been reported for malonaldehyde,[32–35] tropolone[36–49] and its derivatives,[50–54] 9-hydroxyphenalenones,[55–61] and 6-hydroxybenzanthrone.[62]

Analysis of the SVL fluorescence obtained after selective excitation of low-energy transitions allowed detection and assignments of several vibrational levels which were not observed previously. Additional help in the assignment was provided by the doublet structure of the LIF spectra with constant spacing between the two components. The fluorescence spectra obtained for excitation into each of the two tunneling levels of the same vibrations are very similar, but they strongly differ for excitation of different modes. This is crucial for reliable separation of nearby or even overlapping transitions.

Some additional examples of SVL spectra obtained for excitation into different low-frequency vibronic bands are presented in Figure 6. The spectra in Figures 5(b)–5(d) and 6 are very simple and dominated in each case by one prominent band assigned as ν_1^1 type sequence origin. The remaining bands are assigned as $\nu_1^1 x_1^0$ type cross-sequence transitions, where ν and x correspond to two different modes. Only a few modes are active in the spectra built off ν_1^1: they correspond to $2A_g$, $3A_g$, and $4A_g$ totally symmetric vibrations and their combinations; in some cases, weaker intensity transitions in-

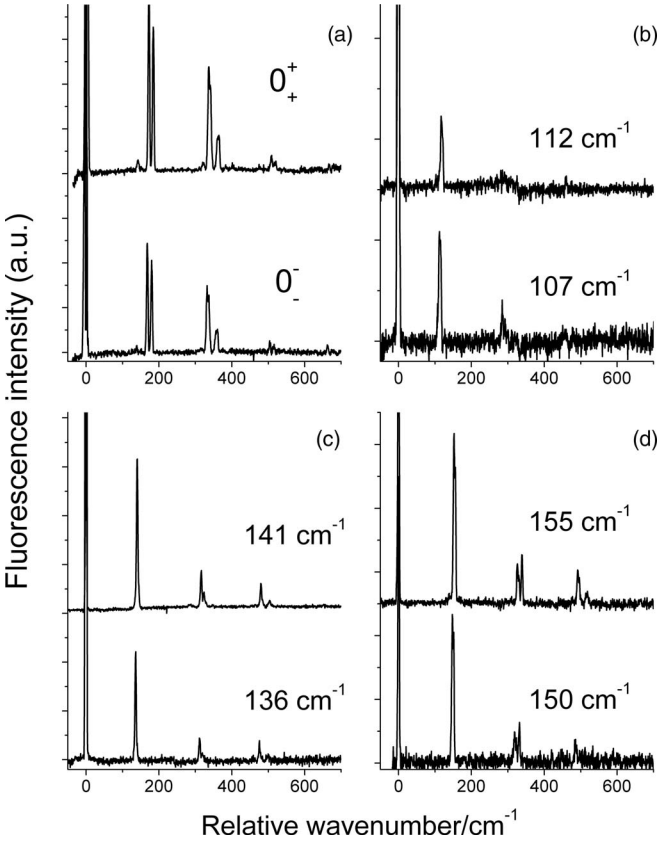

FIG. 5. Comparison of dispersed fluorescence spectra obtained for selective excitation into both components of tunneling doublets: (a) 0^+_+ and 0^-_-, (b) 107/112, (c) 136/141, (d) 150/155 cm^{-1}.

volving $1A_g$ mode are also observed. The same modes dominate the fluorescence recorded from the electronic origin. Also the relative intensities are quite similar. The assignment of vibrations based on 0-0 and single vibronic level emissions is presented in Table I.

Nearly all bands observed in SVL spectra reveal doublet splittings similar to the values of 4-5 cm^{-1} observed in the LIF spectra. Since the spectral resolution of our setup is worse for

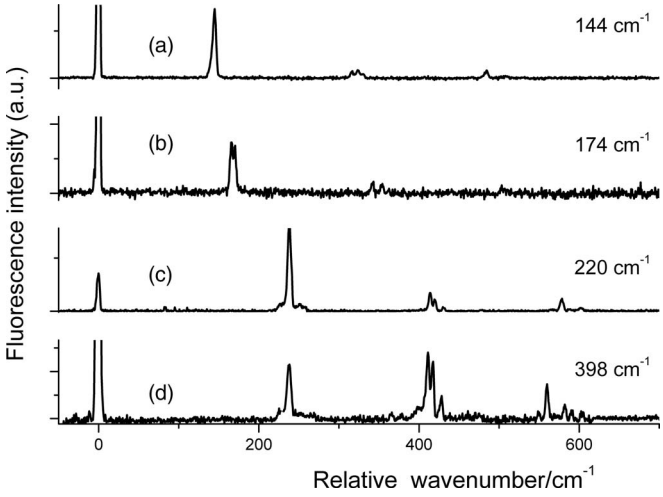

FIG. 6. Dispersed fluorescence spectra obtained for excitation into low-frequency bands: (a) 144 cm^{-1}, (b) 174 cm^{-1}, (c) 220 cm^{-1}, (d) 398 cm^{-1}.

the emission, the doublets are not so well resolved as in the LIF spectra, except for the $2A_g$ mode, its overtones and combinations, for which the splittings exceed 10 cm^{-1}. The observation of a constant spacing between the doublet components in the LIF spectrum allows us to assume a negligible tunneling splitting in S_1. We use the symbols Δ_0 and Δ_i to indicate the S_0 splitting for the vibrationless level and for the v = 1 level of the *i*th mode. Presenting the SVL fluorescence as a function of $\tilde{\nu}_{ex}$ - $\tilde{\nu}_{fl}$, where the former indicates the excitation energy and the latter, the recorded emission intensity, one observes doublets separated by Δ_i. For the excitation from the lower (+) level, the two peaks are located at $f + 1/2(\Delta_0 - \Delta_i)$ and $f + 1/2(\Delta_0 + \Delta_i)$; for the excitation from the upper (−) level the corresponding locations are $f - 1/2(\Delta_0 + \Delta_i)$ and $f + 1/2(\Delta_i - \Delta_0)$. The centers of the doublets are located at $f + \Delta_0/2$ and $f + \Delta_i/2$ for excitation from (+) and (−), respectively. By *f* we denote the (v = 0) → (v = 1) transition energy that would have been observed had there been no splitting. This value should be compared with the calculated vibrational frequency. For a special case of $\Delta_0 = \Delta_i = \Delta$, the tunneling doublets observed in SVL are located at *f* and $f + \Delta$ for excitation from the (+) level, whereas for the excitation originating from (−) they are positioned at $f - \Delta$ and *f*. Given our accuracy of about 1 cm^{-1}, such situation is encountered most frequently. In Table I we present the frequency values obtained for excitation into both the (+) and (−) levels; the former are more reliable because of the greater population of the lower level, which results in higher emission intensity.

Excitation into the higher component of the 107/112 cm^{-1} doublet (Figure 5(b)) gives, in addition to resonance fluorescence peak, a band peaking at 117 cm^{-1} with a shoulder at 121 cm^{-1}. The origin-excited dispersed fluorescence spectrum does not show any vibronic band at this frequency, but a peak was observed at 120 cm^{-1} in the INS spectrum.[27] The calculations for S_0/S_1 predict a vibration of B_g symmetry at 117/107 cm^{-1}. Therefore the 107 cm^{-1} band in the LIF spectrum and the 117 cm^{-1} transition in the emission are assigned to the $1B_g$ mode in the S_1 and S_0 states, respectively.

The fluorescence emission spectrum following the excitation of 136/141 cm^{-1} transition (Figure 5(c)) is also dominated by one prominent band at 140 cm^{-1} acting as sequence origin. This band is absent in the origin-excited dispersed fluorescence spectrum; a feature at 134 cm^{-1} has been observed by INS.[27] The calculations predict for S_1 a fundamental vibration of B_g symmetry at 129 cm^{-1}; the ground state frequency is calculated as 130 cm^{-1}. Therefore, the 136 cm^{-1} band in the LIF spectrum (a lower energy component of a doublet) and the 140 cm^{-1} transition in SVL fluorescence can be assigned to $2B_g$.

Figure 6(a) shows fluorescence emission obtained via excitation of the 0 + 144 cm^{-1} band in the LIF excitation spectrum. The emission is dominated by one prominent band at 145 cm^{-1}. This feature is already observed in the origin-excited fluorescence emission spectrum and assigned as $1A_g$. Weak intensity bands are also observed at 316, 324, 330, 485, and 507 cm^{-1} from the excitation energy. Except for the 330 cm^{-1} band feature (tentatively attributed to $2B_g + 3B_g$), they can be assigned to the combination of $1A_g$ with $2A_g$, $3A_g$, and $4A_g$ modes. Because of a large value of the tunneling splitting for $2A_g$, the two components are clearly resolved. This is not the case for $3A_g$ and $4A_g$, but the presence of doublets can be deduced from the larger widths of these peaks. On the other hand, the peak corresponding to the $1A_g$ mode is narrower. The origin of that may, in principle, be twofold: (i) small value of the tunneling splitting for this mode; (ii) lack of equilibration between "plus" and "minus" S_1 levels on the time scale of S_1 lifetime (ns). The latter is improbable, as we observe emission from both components for modes other than $1A_g$. For the particular case of the $1A_g$ vibration, it has been already demonstrated that it exhibits practically no tunneling splitting.[24] However, we will return to the general problem of equilibration of the two tunneling levels in a separate section.

Dispersed fluorescence emission spectrum following the 0 + 155 cm^{-1} band excitation is presented in Figure 5(d). The spectrum is dominated by a prominent band at 152 cm^{-1}, exhibiting a doublet structure with a separation of 4 cm^{-1}. This band is not observed in the origin-excited dispersed fluorescence. Based on the results of calculations regarding both, the absolute frequencies, as well as the agreement between the predicted and observed shifts between S_0 and S_1, we assign this band to the $2A_u + 3A_u$ combination.

Figure 6(b) shows the emission spectrum obtained for excitation into the 0 + 174 cm^{-1} band. The spectrum is dominated by one prominent sequence origin doublet band at 166/170 cm^{-1}. This band is absent in the origin-excited dispersed fluorescence spectrum. Based on calculations and the agreement between computed and observed frequency changes between S_0 and S_1, we assign it to the first overtone of the $3A_u$ vibration.

Figure 6(c) shows the fluorescence emission spectrum obtained for excitation into the 0 + 220 cm^{-1} band in the LIF excitation spectrum. The spectrum is dominated by one prominent sequence origin at 239 cm^{-1}. Although small in intensity, this band is also observed in the fluorescence emission recorded for origin band excitation. We assign this transition to $2 \times 1B_g$, in excellent agreement with the calculated frequency and the S_1-S_0 shift. This band forms the origin for transitions involving $2A_g$, $3A_g$, and $4A_g$ modes.

Excitation of the 0 + 394/398 cm^{-1} features (Figure 6(d)) gives a similar spectrum to that of 0 + 219 cm^{-1} excitation. Now, however, the intensities of the peaks corresponding to $2 \times 1B_g$ and $2A_g$ are similar. We therefore assign the 0 + 398 cm^{-1} band in the LIF excitation spectrum as the combination of $2A_g + 2 \times 1B_g$.

3. 0_0^0 +184, 362, 364, and 541 cm^{-1} excitations

Figure 7 shows dispersed fluorescence emission spectra obtained following the excitation of 0 + 184, 362 364, and 541 cm^{-1} bands in the LIF spectrum, respectively. Even a cursory glance at the spectra reveals that the spectra in Figures 7(a), 7(b), and 7(d) form a group with a similar pattern, while that presented in Figure 7(c) is completely different.

The spectrum shown in Figure 7(a) is dominated by two bands at 174 and 186 cm^{-1} acting as sequence origin,

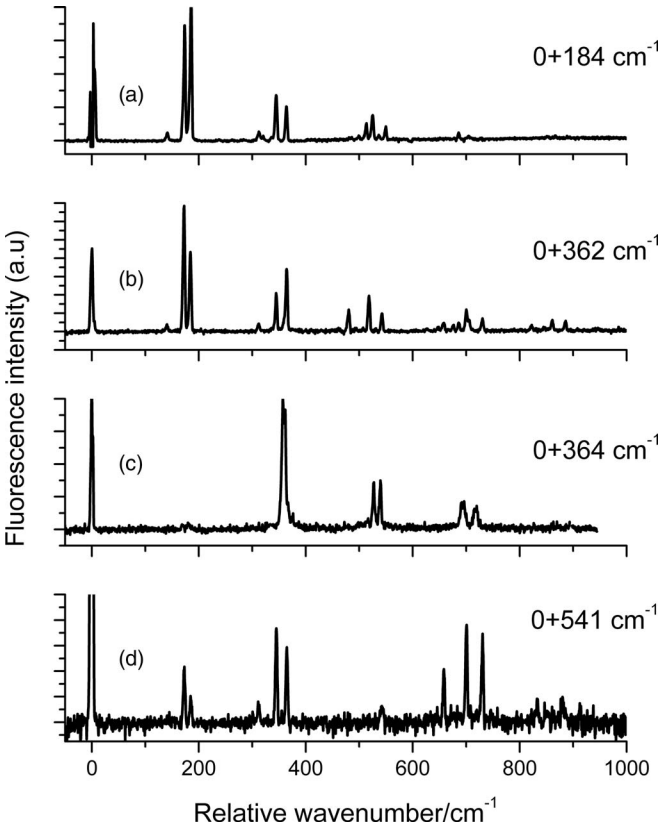

FIG. 7. Dispersed fluorescence spectrum obtained via excitation of (a) 0+184, (b) 0+362, (c) 0+364, and (d) 0 + 541 cm^{-1} bands.

belonging to the tunneling doublet of the $2A_g$ mode. Therefore the band at 0 + 184 cm^{-1} in the LIF excitation spectrum is assigned as $2A_g$. The bands at 143, 324, 514/526, and 538/551 cm^{-1} are also observed in the fluorescence emission spectrum obtained via excitation into the origin and are already assigned as $1A_g$, $1A_g + 2A_g$, $2A_g + 3A_g$, and $2A_g + 4A_g$, respectively.

Two medium intensity bands are located at 345 and 365 cm^{-1}. These frequencies are close to those corresponding to $3A_g$ and $4A_g$ modes, respectively. However, these bands are narrow and do not reveal splitting into doublets, expected for both $3A_g$ and $4A_g$ modes. Therefore, we assign these bands as the overtones of the $2A_g$ mode doublet. Similarly, the bands observed at 525 and 549 cm^{-1} are assigned to the third harmonic progression of the $2A_g$ mode. Of the remaining bands, the 501 cm^{-1} can be assigned to $6B_g$. This transition has been previously observed in the Raman spectrum,[27] but not in fluorescence.

Figure 7(b) shows the emission spectrum following excitation of the 0 + 362 cm^{-1} band in the LIF excitation spectrum. The spectrum exhibits features very similar to those observed in the emission obtained for 0 + 181 cm^{-1} excitation. Therefore, from the similarities of the spectra in Figures 7(a) and 7(b), we assign the 0 + 360 cm^{-1} band in the LIF spectra as the second harmonic of the $2A_g$ mode. One can notice that the number of harmonic progressions of the $2A_g$ mode observed in Figure 7(b) is greater than that in Figure 7(a). Such an increase in intensity and number of vibronic progressions with increasing excitation quanta is observed, e.g, in tolanes.[63] The increase in intensity and number of vibronic progressions can be exploited for modeling the potential energy surface along the mode in consideration. The pairs of bands at 345 and 364 cm^{-1}, 518 and 543 cm^{-1}, 700 and 731 cm^{-1}, and 861 and 886 cm^{-1} are assigned as 2 × 2Ag, 3 × 2Ag, 4 × 2Ag, and 5 × 2Ag progressions, respectively. It is remarkable that the pattern of the intensities of the doublet components is reversed for 184 and 362 cm^{-1} excitations.

Shifting the excitation by merely 2 cm^{-1}, to 0 + 364 cm^{-1}, results in a dramatic change in the SVL spectrum (Figure 7(c)). It is now dominated by the $4A_g$ band. The features around 170/180 cm^{-1} are barely detected, but the $2A_g$ mode is readily observed at 527/540 cm^{-1}: this band doublet corresponds to the $4A^1_{g1}2A^0_{g1}$ transition. Contributions from $3A_g$ and $4A_g$ are also observed at 696 and 720 cm^{-1}. Comparison of two completely different spectra obtained for very similar excitation energies reveals the power of SVL experiments in disentangling complicated spectral patterns.

Figure 7(d) shows the fluorescence emission spectrum obtained for excitation of the 0 + 541 cm^{-1} band in the LIF excitation spectrum. The emission reveals features similar to those of Figures 7(a) and 7(b), but is relatively simpler. Interestingly, while the vibronic activity in the vicinity of $3 \times 2A_g$ is extremely weak, all the other vibronic progressions of the $2A_g$ mode are observed. Therefore, we assign the band at 0 + 541 cm^{-1} in the LIF excitation spectra to $3 \times 2A_g$. The low intensity of the $2A^3_{g3}$ transition can be due to the interaction between nearly isoenergetic $3 \times 2A_g$ and $2A_g + 4A_g$ levels in the ground electronic state.

4. 0^0_0 +339, 364, 400, 481, and 518 cm^{-1} excitations

Figures 8(a)–8(d) presents dispersed fluorescence emission recorded for excitation into the 0+339, 364, 400, and 481 cm^{-1} bands in the LIF excitation spectrum. The corresponding sequence origins are observed in the emission spectra at 337, 361, 398, and 481 cm^{-1}.

All bands except 400 cm^{-1} are already observed in the origin-excited dispersed fluorescence emission spectrum. The Raman spectra yielded a feature at 399 cm^{-1}, assigned to $5B_g$.[27] All the spectra show similar features in that all are dominated by one prominent sequence origin, while the rest of the bands belong to vibrations observed also for excitation into the origin. Thus the bands at 0 + 339, 364, 400, and 481 cm^{-1} in the LIF excitation spectrum are assigned as $3A_g$, $4A_g$, $5B_g$, and $5A_g$, respectively.

Figure 8(e) shows the emission spectrum for excitation into the 0 + 518 cm^{-1} band in the LIF spectrum. This spectrum looks different from the others in that there is no dominant band. However, the doublet at 343/348 cm^{-1} belonging to $3A_g$ and its combination with $2A_g$ at 514 and 526 cm^{-1} seems to compete for sequence origin. The analysis of the bands in this spectrum leads to the assignment of the band at 518 cm^{-1} in the LIF spectrum as the combination of $2A_g + 3A_g$.

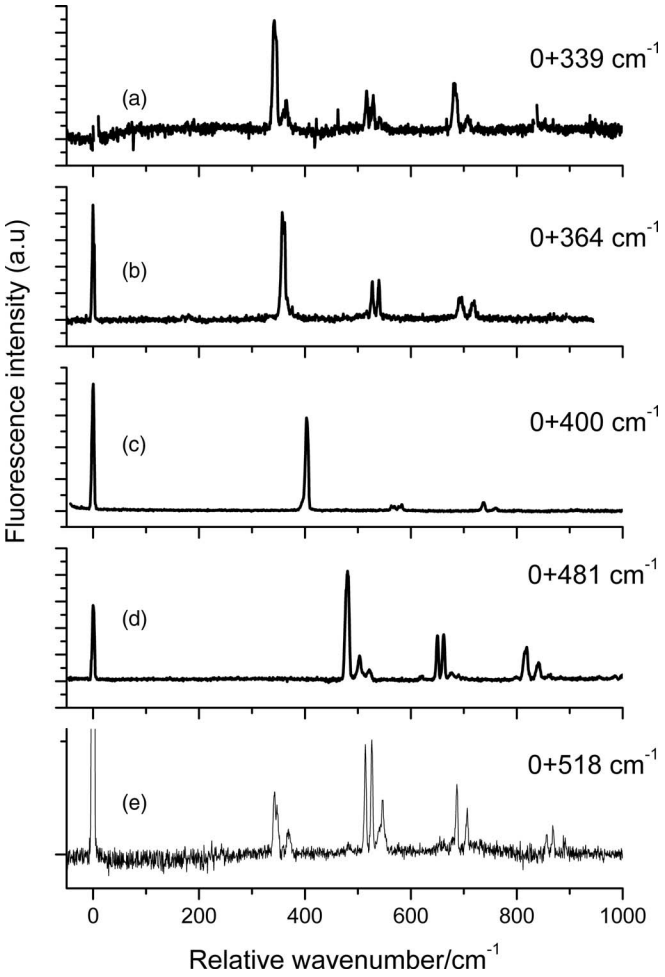

FIG. 8. Dispersed fluorescence spectrum obtained for excitation into (a) 0 + 339, (b) 0 + 364, (c) 0 + 400, (d) 0 + 481, and (e) 0 + 519 cm^{-1} bands.

5. 0_0^0 +826, 909, and 951 cm^{-1} excitations

The corresponding spectra are shown in Figures 9(a)–9(c). All the spectra show similar features among themselves, but very different from the rest of the emission spectra discussed so far. They are characterized by broad and redshifted emission, a characteristic signature of IVR.[31] It has already been pointed out that the LIF excitation spectrum suggests complicated excited state dynamics for excitation beyond 800 cm^{-1} above the 0-0 transition. The single vibronic level fluorescence emission spectra presented in this section confirm this conjecture. In Figure 9(a), one can see a few discrete vibronic bands which could suggest a restricted IVR, while Figures 9(b) and 9(c) show very broad emissions, characteristic of dissipative IVR. Due to complex dynamics of porphycene excited with 800 cm^{-1} or higher excess energy above the 0-0 transition, it was not possible to clearly assign the vibronic bands in the LIF excitation spectrum in this case.

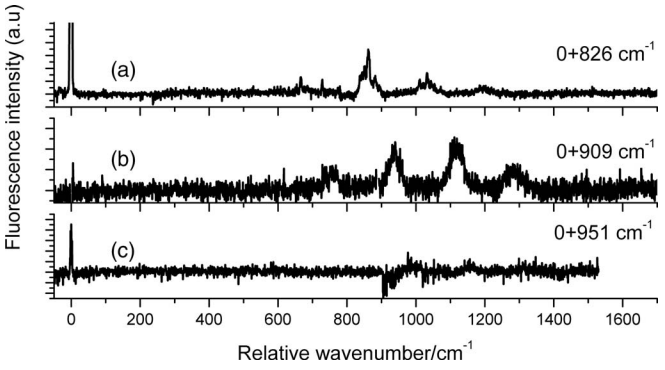

FIG. 9. Dispersed fluorescence spectra obtained via excitation of (a) 0 + 826 cm^{-1}, (b) 0 + 909 cm^{-1}, and (c) 0 + 951 cm^{-1} bands.

C. Comparison between experimental and calculated frequencies

The analysis of SVL spectra allowed us to assign the origin of vibronic bands observed in the excitation and emission spectra of porphycene. Table I presents the assignment of over a hundred peaks (fifty doublets) observed in the LIF excitation spectrum in the range up to 850 cm^{-1}. The analysis reveals the dominant role of totally symmetric modes, of which $2A_g$ is particularly active. Among the non-totally symmetric modes, $1B_g$ and $2B_g$ are present as fundamentals, combinations and overtones. A previously non-observed $3B_g$ mode was detected, both in LIF (combination with $2B_g$) and in emission (as a fundamental). Other modes observed for the first time are $1A_u$, $2A_u$, and $3A_u$; they were detected as combinations or overtones.

Optimization of geometry, followed by calculation of vibrational frequencies was performed for porphycene in both S_0 and S_1 electronic states. Figure 10 and Table II present the comparison between theory and experiment. Except for one mode in the S_1 state ($5B_g$) the agreement between theory and experiment is perfect. Practically the same fit quality is obtained for 6-31G(d,p) and 6-311++G(d,p) basis sets. For the ground state calculations, the double-zeta/triple zeta basis sets yield the scaling factor of 0.9802/0.9863, correlation coefficient r = 0.99983/0.99980, and the root mean square error of 8/9 cm^{-1}. For the S_1 calculations the corresponding values are 0.9902/0.9960, 0.99944/0.9993, and 12/13 cm^{-1}. Closer analysis reveals that not only the $5B_g$ mode in S_1, but, in general, other out-of-plane vibrational transitions are calculated with worse accuracy than the in-plane modes, both for S_0 and S_1. We have recently extensively discussed this finding on the example of another planar aromatic molecule, 1H-pyrrolo[3,2-*h*]quinoline.[64]

D. Dynamics of intramolecular energy flow

The fact that the vibronic levels are split due to tunneling provides an opportunity to trace the relaxation of the initially excited levels by looking at the relative intensities of the doublet components. In most cases, selective excitation into either component of a tunneling doublet results in the emission from both (+) and (−) levels, demonstrating efficient equilibration on the time scale of S_1 lifetime. It should be recalled that the tunneling splittings in S_1 are small, of the order of a fraction of a wavenumber.[24] In order to evaluate the rate constant for equilibration, we carried out time-resolved experiments, searching for a possible delay between the

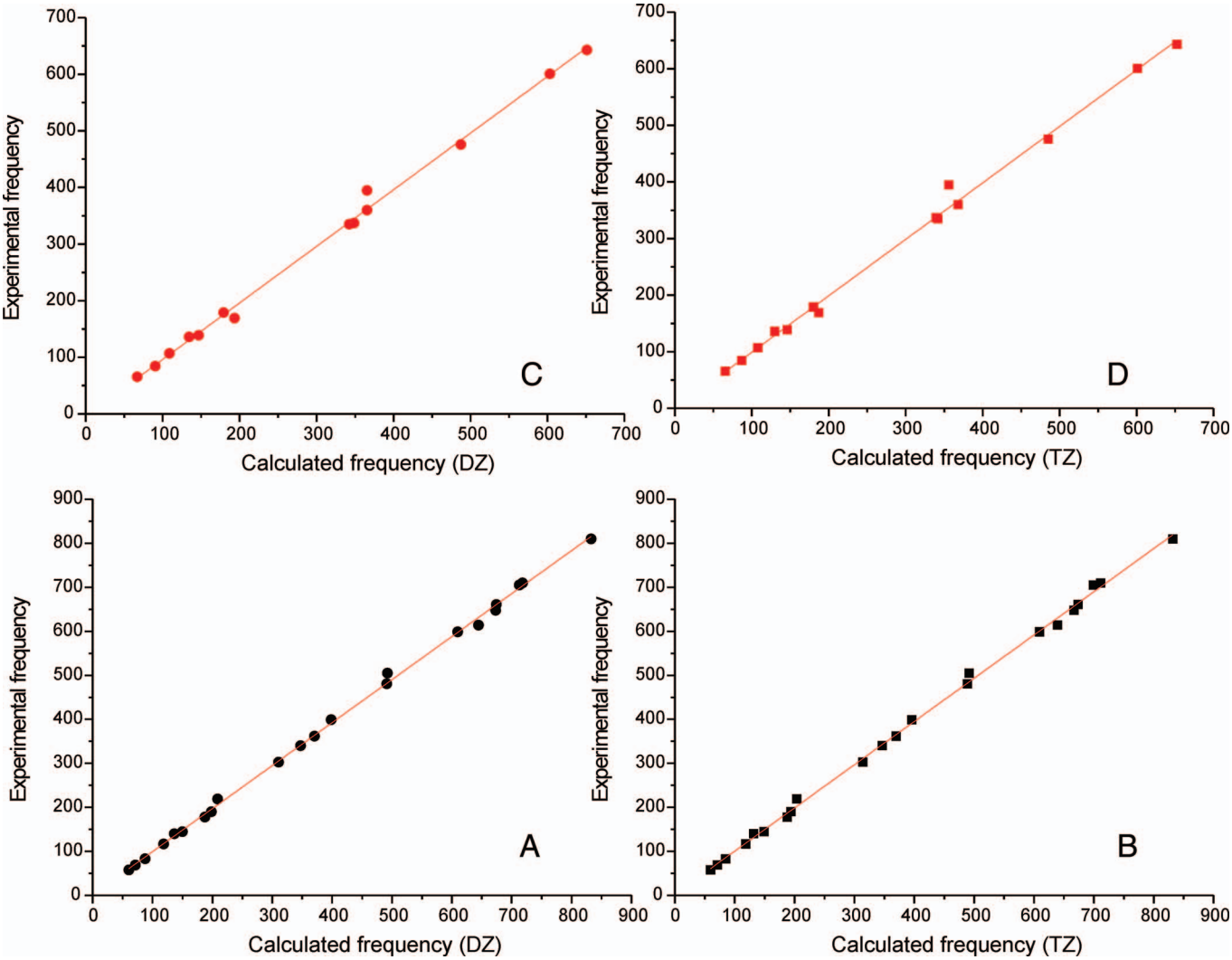

FIG. 10. Comparison of experimental and calculated vibrational modes of porphycene in the ground (bottom) and the lowest excited singlet state (top). A and C, B3LYP/6-31G(d,p), B and D, B3LYP/6-311++G(d,p) calculations. The plots for S_0 include also the $8A_g$ mode at 810 cm^{-1},[27] not observed in the present work.

onset of two emissions. No such delay could be determined while exciting into the origin. The time resolution of our oscilloscope is about 1 ns, implying that the relaxation rate is above 10^9 s^{-1}. Since the expected fluorescence lifetime is above 10 ns, the molecules excited into the origin can fully relax. The situation may be different for excitation into higher vibronic levels. As already discussed, the emission spectra change significantly for the excess energy above 800 cm^{-1}.

For lower frequency vibrations the relaxation seems to be efficient. However, closer inspection of the spectra reveals remarkable exceptions, in particular for low-frequency modes. For the $2A_g$ pair, the relative intensities are practically the same no matter whether lower (179 cm^{-1}) or upper (184 cm^{-1}) tunneling pair is excited. This is not the case for $1B_g$ and $2B_g$ doublets (107/112 and 136/141 cm^{-1}, respectively) for which the emission occurs from the initially excited levels (Figure 5).

An interesting alternation of relative intensities is observed for the progressions of the $2A_g$ vibration, the mode which exhibits the largest splitting. It is also the most active mode in the fluorescence spectra. Because of considerable spectral separation of the doublet components of this mode and its activity, this vibration can be analyzed in detail by inspection of the SVL spectra, discussed in Sec. III E.

E. Mode-selective and vibrational-level-dependent tunneling splittings

Both supersonic jet[23] and helium nanodroplets[24] studies demonstrated that tunneling splitting in porphycene is mode-selective. The largest value of the splitting, 12 cm^{-1}, is observed for the $2A_g$ mode and its combinations with $3A_g$ and $4A_g$, for the $1A_g$ and $7A_g$ vibrations the splitting is negligibly low, whereas for other modes ($3A_g$, $4A_g$, $2 \times 3A_g$, $3A_g + 4A_g$) the values are similar to that observed for the zero-point energy level, 4.4 cm^{-1}. Our present results allow us to determine the values of tunneling splitting for the states in which two ground state vibrations are simultaneously excited, as well as to observe the values for different excitation levels of a particular mode. Due to the spectral resolution of our instrument, we could reliably monitor the changes

TABLE II. Comparison of experimental and calculated low frequency modes of porphycene in S_0 and S_1 electronic states. The calculated values include scaling factors (see text).

S_0			S_1			
Expt.	6-31G(d,p)	6-311++G(d,p)	Expt.	6-31G(d,p)	6-311++G(d,p)	Assignment
58	60	59	…	55	54	$1A_u$
69	71	70	65,5	66	65	$2A_u$
83	87	84	84,5	90	87	$3A_u$
117	116	117	107	108	107	$1B_g$
140	133	130	136	133	129	$2B_g$
145	147	147	139	145	146	$1A_g$
178	184	185	179	177	179	$2A_g$
190	194	191	169	191	186	$3B_g$
219	204	201	…	…	…	$4B_g$
303	311	310	283[a]	284	290	$5A_u$
340	340	342	335	339	340	$3A_g$
362	363	365	360	362	367	$4A_g$
399	390	390	395	362	355	$5B_g$
481	482	482	476	483	483	$5A_g$
505	483	485	…	…	…	$6B_g$
614	632	630	…	…	…	$7B_g$
599	598	601	601	597	599	$6A_g$
648	660	658	…	…	…	$8B_g$
661	661	664	643	645	650	$7A_g$
705	699	690	…	…	…	$9B_g$
710	704	702	…	…	…	$10B_g$
810	816	820	…	…	…	$8A_g$

[a]Estimated assuming 54 cm^{-1} for the frequency of $1A_u$.

in the $2A_g$ mode, the one that exhibits the largest splitting. Table III shows the values obtained for coexcitation of different S_0 vibrational levels. Two important features are evident. The first is the lowering of tunneling splitting of $2A_g$ for states in which, in addition to this mode, another vibration is excited. This was found for $1A_g$, $1B_g$, and $2B_g$ modes. The forms of these modes are shown in Figure 11. In our previous Car-Parrinello molecular dynamics study of tautomerism in porphycene, simulation of simultaneous excitation was performed for $1A_g$, the "inhibiting" mode which reveals no tunneling splitting and $2A_g$, the "enhancing" mode with a large splitting.[25] The results indicated that the enhancing nature of $2A_g$ prevails over the inhibiting character of $1A_g$. This is in line with the present finding, since the tunneling splitting of 8 cm^{-1} measured for the $1A^1_{g1}2A^0_{g1}$ transition is significantly higher than the value of 4.4 cm^{-1} observed for the vibrationless level. Regarding $1B_g$ and $2B_g$ modes, their out-of-plane character could suggests weakening of intramolecular hydrogen bonds during vibrational motion, which should result in a smaller splitting. Our spectral resolution is too small to verify this by looking directly at these modes, not at combinations, but a splitting somewhat smaller than 5 cm^{-1} and the lack of splitting observed for $1B_g$ and $2 \times 1B_g$ excitations, respectively, suggest it may be the case.

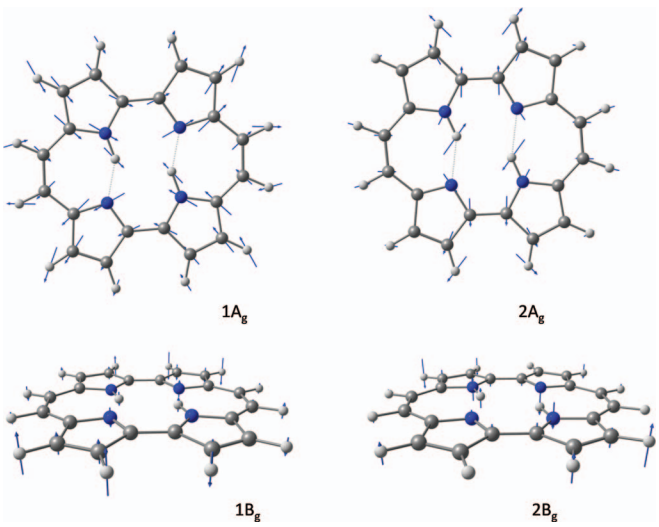

FIG. 11. Displacement vectors of $1A_g$, $2A_g$, $1B_g$, and $2B_g$ normal modes, obtained using B3LYP/6-311++G(d,p) calculations.

The second characteristic feature is a substantial increase of tunneling splitting for the overtones of $2A_g$. The values of 12, 20, and 24 cm^{-1} have been obtained for $v = 1$, 2, and 3, respectively, which shows the crucial character played by this mode in the tautomerization path. Moreover, large values of the splitting allow us to hope that reliable splitting values can be obtained for porphycene with one or perhaps even two internal protons exchanged for deuterons.

Table III also shows that the relative intensities of the bands forming tunneling doublets vary quite strongly, depending not only on excitation, i.e., the upper level, but also on the lower one. In particular, observation of S_0 overtones of $2A_g$ (Figures 7(a) and 7(b)) reveals the reversal of intensities for transitions ending on $v = 1$ and $v = 2$. Moreover, the reversal is also observed for a particular ground state vibrational level when the excited state level changes from $v = 1$ to $v = 2$.

TABLE III. Ground state tunneling splitting of the $2A_g$ mode obtained from SVL spectra for different vibrationally excited levels.

Excitation[a]	Transition	Tunneling splitting (cm^{-1})	Relative intensities [b] I_{low}/I_{high}
0^-	$2A^0_{g1}$	12	1.3
0^+	$2A^0_{g1}$	12	1.2
136	$2A^0_{g1}2B^1_{g1}$	7	2.1
141	$2A^0_{g1}2B^1_{g1}$	7	2.0
144	$1A^1_{g1}2A^0_{g1}$	8	0.9
155	$2A^0_{g1}2A^1_{u1}3A^1_{u1}$	13	0.8
179	$2A^1_{g1}$	12	0.9
184	$2A^1_{g1}$	12	0.8
220	$2A^0_{g1}1B^2_{g1}$	6	1.8
335	$2A^0_{g1}3A^1_{g1}$	12	1.2
339	$2A^0_{g1}3A^1_{g1}$	13	1.2
360	$2A^0_{g1}4A^1_{g1}$	13	1.1
362	$2A^2_{g1}$	12	1.6
362	$2A^2_{g2}$	20	0.5
362	$2A^2_{g3}$	24	2.0
364	$2A^0_{g1}4A^1_{g1}$	12	1.2
476	$2A^0_{g1}5A^1_{g1}$	11	1.2
481	$2A^0_{g1}5A^1_{g1}$	12	0.9
514	$2A^1_{g1}3A^1_{g1}$	13	0.6
514	$2A^1_{g2}3A^1_{g1}$	20	0.9
518	$2A^1_{g1}3A^1_{g1}$	12	0.9
518	$2A^1_{g2}3A^1_{g1}$	20	1.2
521	$2A^1_{g1}1A^1_{u1}5A^1_{u1}$	15	2.1
532	$2A^1_{g1}1B^2_{g2}2B^1_{g1}$	15	1.7
532	$2A^1_{g2}1B^2_{g2}2B^1_{g1}$	20	1.8
541	$2A^3_{g1}$	12	2.0
541	$2A^3_{g2}$	20	1.2

[a]Excess energy (cm^{-1}) counted from 0^-.
[b]Indices low/high correspond to the transition energy of $2A_g$ doublet components; estimated maximum error: ±30%.

These findings may be interpreted as indicating different energy order of (+) and (−) levels for even and odd vibrational quantum numbers.

IV. SUMMARY AND CONCLUSIONS

Measurements of LIF excitation in combination with hole burning spectroscopy have revealed several transitions which have never been reported so far. Due to the lack of a simple one-to-one correlation between the LIF excitation and dispersed fluorescence spectrum of porphycene excited into the S_0-S_1 electronic origin, we have recorded single vibronic level fluorescence spectra. Combined with quantum chemical calculations, this procedure led to the precise assignment of low frequency vibrations of porphycene in the S_1 state. Almost all the single vibronic level fluorescence emissions give a simple pattern dominated by one sequence origin band, which makes the assignment and correlation of the vibronic bands in the S_0 and S_1 states pretty straightforward. Comparison of the spectroscopic characteristics of the tunneling doublets of the origin band has also been investigated. In most cases, the spectra of the doublets are similar, except for the 4-5 cm^{-1} characteristic redshift. Our single vibronic level fluorescence study also shows that the excited state dynamics is dominated by IVR for 800 cm^{-1} or higher excess energy above the S_1 origin. Based on single vibronic level fluorescence study in combination with quantum chemical calculations, we are able to unambiguously assign the S_1 vibrations of porphycene and correlate the vibrations in S_0 and S_1 states. The comparison shows that the S_1 vibrational frequencies are generally smaller than their S_0 counterparts. Moreover, our results demonstrate that the low frequency vibrations in the electronically excited S_1 state can now be computed with the accuracy comparable to that of the ground state.

It turned out that the excitation into each of the two tunneling doublets leads to similar spectroscopic features. Guided by the spectroscopic similarity and the characteristic redshifts, we were able to identify and compare the spectroscopic characteristics of various pairs of tunneling doublets, using selective excitation into the bands observed in the LIF excitation spectrum. For several cases, coupling of the $2A_g$ mode with other vibrations was observed, resulting in the lowering of tunneling splitting. Most interesting, the tunneling splitting of the $2A_g$ mode was found to strongly increase in higher S_0 vibrational levels. Since $2A_g$ mode is considered crucial for the promotion of tautomerization in porphycene,[20,25,65] more detailed investigations are now underway, involving singly and doubly deuterated species. These studies may lead to a better understanding of the multidimensional character of doubly hydrogen transfer in porphycene.

In summary, porphycene provides a very good model for studying the vibrational mode dependence of tunneling splitting. This area has been intensely exploited so far for malonaldehyde,[35,66–74] tropolone,[40–42,48,49,54,75–91] and 9-hydroxyphenalenone.[60,92–94] Tunneling in these systems involves one proton, whereas in porphycene two protons are delocalized. This makes porphycene a unique system for studying such aspects of tunneling as synchronous vs. stepwise mechanism or the role of cooperativity.

ACKNOWLEDGMENTS

This work was supported by grants from the Polish Ministry of Science and Higher Education (Grant No. NN 204264238) and from National Science Centre (Grant No. DEC-2011/02/A/ST5/00443). J.S. and E.M. acknowledge the International Ph.D. Projects Program co-financed by the Foundation for Polish Science and the European Regional Development Fund within the Innovative Economy Operational Program, "Grants for Innovation." We acknowledge a computing grant from the Interdisciplinary Centre for Mathematical and Computational Modeling.

[1]E. Vogel, M. Köcher, H. Schmickler, and J. Lex, Angew. Chem., Int. Ed. Engl. **25**, 257 (1986).
[2]D. Sánchez-Garcia and J. L. Sessler, Chem. Soc. Rev. **37**, 215 (2008).
[3]S. E. Braslavsky, M. Müller, D. O. Mártire, S. Pörting, S. G. Bertolotti, S. Chakravorti, G. Koç-Weier, B. Knipp, and K. Schaffner, J. Photochem. Photobiol., B **40**, 191 (1997).
[4]J. C. Stockert, M. Cañete, A. Juarranz, A. Villanueva, R. W. Horobin, J. Borrell, J. Teixidó, and S. Nonell, Curr. Med. Chem. **14**, 997 (2007).

[5]J. Waluk, in *CRC Handbook of Organic Photochemistry and Photobiology*, edited by M. Oelgemoeller, A. Griesbeck, and F. Ghetti (Taylor and Francis, 2011).
[6]J. Waluk, in *Handbook of Porphyrin Science*, edited by K. Smith, K. Kadish, and R. Guilard (World Scientific, Singapore, 2010), Vol. 7, p. 359.
[7]J. Waluk, in *Hydrogen-Transfer Reactions*, edited by J. T. Hynes, J. P. Klinman, H. H. Limbach, and R. L. Schowen (Wiley-VCH, Weinheim, 2007), Vol. 1, p. 245.
[8]C. Richert, J. M. Wessels, M. Müller, M. Kisters, T. Benninghaus, and A. E. Goetz, J. Med. Chem. **37**, 2797 (1994).
[9]S. Nonell, N. Bou, J. I. Borrell, J. Teixidó, A. Villanueva, A. Juarranz, and M. Cañete, Tetrahedron Lett. **36**, 3405 (1995).
[10]C. Milanesi, R. Biolo, G. Jori, and K. Schaffner, Lasers Med. Sci. **6**, 437 (1991).
[11]N. K. Mak, T. W. Kok, R. N. S. Wong, S. W. Lam, Y. K. Lau, W. N. Leung, N. H. Cheung, D. P. Huang, L. L. Yeung, and C. K. Chang, J. Biomed. Sci. **10**, 418 (2003).
[12]D. Baumer, M. Maier, R. Engl, R. M. Szeimies, and W. Bäumler, Chem. Phys. **285**, 309 (2002).
[13]B. Wehrle, H. H. Limbach, M. Köcher, O. Ermer, and E. Vogel, Angew. Chem., Int. Ed. Engl. **26**, 934 (1987).
[14]J. Braun, M. Schlabach, B. Wehrle, M. Köcher, E. Vogel, and H. H. Limbach, J. Am. Chem. Soc. **116**, 6593 (1994).
[15]J. Sepioł, Y. Stepanenko, A. Vdovin, A. Mordziński, E. Vogel, and J. Waluk, Chem. Phys. Lett. **296**, 549 (1998).
[16]P. Fita, P. Garbacz, M. Nejbauer, C. Radzewicz, and J. Waluk, Chem.-Eur. J. **17**, 3672 (2011).
[17]M. Gil, J. Dobkowski, G. Wiosna-Sałyga, N. Urbańska, P. Fita, C. Radzewicz, M. Pietraszkiewicz, P. Borowicz, D. Marks, M. Glasbeek, and J. Waluk, J. Am. Chem. Soc. **132**, 13472 (2010).
[18]H. Piwoński, A. Hartschuh, N. Urbańska, M. Pietraszkiewicz, J. Sepioł, A. Meixner, and J. Waluk, J. Phys. Chem. C **113**, 11514 (2009).
[19]P. Fita, N. Urbańska, C. Radzewicz, and J. Waluk, Chem.-Eur. J. **15**, 4851 (2009).
[20]M. Gil and J. Waluk, J. Am. Chem. Soc. **129**, 1335 (2007).
[21]J. Waluk, Acc. Chem. Res. **39**, 945 (2006).
[22]H. Piwoński, C. Stupperich, A. Hartschuh, J. Sepioł, A. Meixner, and J. Waluk, J. Am. Chem. Soc. **127**, 5302 (2005).
[23]A. Vdovin, J. Sepioł, N. Urbańska, M. Pietraszkiewicz, A. Mordziński, and J. Waluk, J. Am. Chem. Soc. **128**, 2577 (2006).
[24]A. Vdovin, J. Waluk, B. Dick, and A. Slenczka, ChemPhysChem **10**, 761 (2009).
[25]Ł. Walewski, J. Waluk, and B. Lesyng, J. Phys. Chem. A **114**, 2313 (2010).
[26]K. Malsch and G. Hohlneicher, J. Phys. Chem. A **101**, 8409 (1997).
[27]S. Gawinkowski, Ł. Walewski, A. Vdovin, A. Slenczka, S. Rols, M. R. Johnson, B. Lesyng, and J. Waluk, Phys. Chem. Chem. Phys. **14**, 5489 (2012).
[28]H. Iga, T. Isozaki, T. Suzuki, and T. Ichimura, J. Phys. Chem. A **111**, 5981 (2007).
[29]T. Isozaki, K. Sakeda, T. Suzuki, and T. Ichimura, J. Chem. Phys. **126**, 214304 (2007).
[30]T. Isozaki, T. Suzuki, and T. Ichimura, Chem. Phys. Lett. **449**, 63 (2007).
[31] G. N. Patwari and S. Wategaonkar, Proc. Indian Natn. Sci. Acad. **69A**, 61 (2003).
[32]C. J. Seliskar and R. E. Hoffmann, J. Mol. Spectrosc. **88**, 30 (1981).
[33]S. L. Baughcum, Z. Smith, E. B. Wilson, and R. W. Duerst, J. Am. Chem. Soc. **106**, 2260 (1984).
[34]C. Duan and D. Luckhaus, Chem. Phys. Lett. **391**, 129 (2004).
[35]T. N. Wassermann, D. Luckhaus, S. Coussan, and M. A. Suhm, Phys. Chem. Chem. Phys. **8**, 2344 (2006).
[36]R. L. Redington and T. E. Redington, J. Mol. Spectrosc. **78**, 229 (1979).
[37]R. Rossetti and L. E. Brus, J. Chem. Phys. **73**, 1546 (1980).
[38]Y. Tomioka, M. Ito, and N. Mikami, J. Phys. Chem. **87**, 4401 (1983).
[39]H. Sekiya, Y. Nagashima, and Y. Nishimura, Bull. Chem. Soc. Jpn. **62**, 3229 (1989).
[40]R. L. Redington, J. Chem. Phys. **92**, 6447 (1990).
[41]H. Sekiya, Y. Nagashima, and Y. Nishimura, J. Chem. Phys. **92**, 5761 (1990).
[42]H. Sekiya, H. Hamabe, H. Ujita, N. Nakano, and Y. Nishimura, J. Chem. Phys. **103**, 3895 (1995).
[43]R. K. Frost, C. Hagemeister, C. A. Arrington, T. S. Zwier, and K. D. Jordan, J. Chem. Phys. **105**, 2595 (1996).
[44]T. Ikoma, K. Akiyama, S. Tero-Kubota, and Y. Ikegami, J. Chem. Phys. **111**, 6875 (1999).
[45]A. E. Bracamonte and P. H. Vaccaro, J. Chem. Phys. **120**, 4638 (2004).
[46]R. L. Redington and T. E. Redington, J. Chem. Phys. **122**, 124304 (2005).
[47]J. C. Keske, W. Lin, W. C. Pringle, S. E. Novick, T. A. Blake, and D. F. Plusquellic, J. Chem. Phys. **124**, 074309 (2006).
[48]R. L. Redington, T. E. Redington, and R. L. Sams, J. Phys. Chem. A **112**, 1480 (2008).
[49]D. Murdock, L. A. Burns, and P. H. Vaccaro, Phys. Chem. Chem. Phys. **12**, 8285 (2010).
[50]H. Sekiya, H. Takesue, Y. Nishimura, Z. H. Li, A. Mori, and H. Takeshita, Chem. Lett. **17**, 1601 (1988).
[51]H. Sekiya, H. Takesue, Y. Nishimura, Z. H. Li, A. Mori, and H. Takeshita, J. Chem. Phys. **92**, 2790 (1990).
[52]T. Tsuji, H. Sekiya, Y. Nishimura, R. Mori, A. Mori, and H. Takeshita, J. Chem. Phys. **97**, 6032 (1992).
[53]H. Sekiya, H. Hamabe, T. Nakajima, A. Mori, H. Takeshita, and Y. Nishimura, Chem. Phys. Lett. **224**, 563 (1994).
[54]K. Nishi, H. Sekiya, H. Kawakami, A. Mori, and Y. Nishimura, J. Chem. Phys. **109**, 1589 (1998).
[55]R. Rossetti, R. C. Haddon, and L. E. Brus, J. Am. Chem. Soc. **102**, 6913 (1980).
[56]R. Rossetti, R. Rayford, R. C. Haddon, and L. E. Brus, J. Am. Chem. Soc. **103**, 4303 (1981).
[57]V. E. Bondybey, R. C. Haddon, and J. H. English, J. Chem. Phys. **80**, 5432 (1984).
[58]H. Sekiya, N. Nakano, K. Nishi, H. Hamabe, T. Sawada, M. Tashiro, and Y. Nishimura, Chem. Lett. **24**, 893 (1995).
[59]K. Nishi, H. Sekiya, H. Hamabe, Y. Nishimura, T. Mochida, and T. Sugawara, Chem. Phys. Lett. **257**, 499 (1996).
[60]K. Nishi, H. Sekiya, T. Mochida, T. Sugawara, and Y. Nishimura, J. Chem. Phys. **112**, 5002 (2000).
[61]T. Matsuo, S. Baluja, Y. Koike, M. Ohama, T. Mochida, and T. Sugawara, Chem. Phys. Lett. **342**, 22 (2001).
[62]G. D. Gillispie, B. M. H. Van, and M. Vangsness, J. Phys. Chem. **90**, 2596 (1986).
[63]K. Okuyama, T. Hasegawa, M. Ito, and N. Mikami, J. Phys. Chem. **88**, 1711 (1984).
[64]A. Gorski, S. Gawinkowski, J. Herbich, O. Krauss, B. Brutschy, R. P. Thummel, and J. Waluk, J. Phys. Chem. A **116**, 11973 (2012).
[65]M. F. Shibl, M. Pietrzak, H. H. Limbach, and O. Kühn, ChemPhysChem **8**, 315 (2007).
[66]T. Hammer and U. Manthe, J. Chem. Phys. **136**, 054105 (2012).
[67]Z. Smedarchina, W. Siebrand, and A. Fernandez-Ramos, J. Chem. Phys. **137**, 224105-1 (2012).
[68]T. Hammer, M. D. Coutinho-Neto, A. Viel, and U. Manthe, J. Chem. Phys. **131**, 224109-1 (2009).
[69]A. Hazra, J. H. Skone, and S. Hammes-Schiffer, J. Chem. Phys. **130**, 054108-1 (2009).
[70]N. O. B. Lüttschwager, T. N. Wassermann, S. Coussan, and M. A. Suhm, Phys. Chem. Chem. Phys. **12**, 8201 (2010).
[71]J. O. Richardson and S. C. Althorpe, J. Chem. Phys. **134**, 054109-1 (2011).
[72]M. Schroeder, F. Gatti, and H.-D. Meyer, J. Chem. Phys. **134**, 234307-1 (2011).
[73]K. Yagi, G. V. Mil'nikov, T. Taketsugu, K. Hirao, and H. Nakamura, Chem. Phys. Lett. **397**, 435 (2004).
[74]V. A. Benderskii, E. V. Vetoshkin, I. S. Irgibaeva, and H. P. Trommsdorff, Russ. Chem. Bull. **50**, 1148 (2001).
[75]D. Murdock, L. A. Burns, and P. H. Vaccaro, J. Chem. Phys. **127**, 081101-1 (2007).
[76]R. L. Redington, J. Chem. Phys. **113**, 2319 (2000).
[77]R. L. Redington, T. E. Redington, T. A. Blake, R. L. Sams, and T. J. Johnson, J. Chem. Phys. **122**, 224311-1 (2005).
[78]R. L. Redington, T. E. Redington, and J. M. Montgomery, J. Chem. Phys. **113**, 2304 (2000).
[79]R. L. Redington, T. E. Redington, and R. L. Sams, Z. Phys. Chem. **222**, 1197 (2008).
[80]M. J. Wójcik, M. Boczar, and L. Boda, J. At., Mol., Opt. Phys. **2012**, 985490 (2012).
[81]M. J. Wójcik, L. Boda, and M. Boczar, J. Chem. Phys. **130**, 164306-1 (2009).
[82]M. J. Wójcik, H. Nakamura, S. Iwata, and W. Tatara, J. Chem. Phys. **112**, 6322 (2000).
[83]K. Nishi, H. Sekiya, H. Kawakami, A. Mori, and Y. Nishimura, J. Chem. Phys. **111**, 3961 (1999).

[84]H. Hamabe, T. Fukuchi, S. Shiraishi, K. Nishi, Y. Nishimura, T. Tsuji, N. Nishi, and H. Sekiya, J. Phys. Chem. A **102**, 3880 (1998).
[85]T. Tsuji, Y. Hayashi, H. Sekia, H. Hamabe, Y. Nishimura, H. Kawakami, and A. Mori, Chem. Phys. Lett. **278**, 49 (1997).
[86]Z. Smedarchina, W. Siebrand, and M. Z. Zgierski, J. Chem. Phys. **104**, 1203 (1996).
[87]S. Takada and H. Nakamura, J. Chem. Phys. **102**, 3977 (1995).
[88]F. A. Ensminger, J. Plassard, and T. S. Zwier, J. Phys. Chem. **97**, 4344 (1993).
[89]H. Sekiya, Y. Nagashima, Y. Nishimura, A. Mori, and H. Takeshita, Chem. Lett. **20**, 237 (1991).
[90]R. L. Redington and C. W. Bock, J. Phys. Chem. **95**, 10284 (1991).
[91]R. L. Redington, Y. Chen, G. J. Scherer, and R. W. Field, J. Chem. Phys. **88**, 627 (1988).
[92]A. Fernandez-Ramos, Z. Smedarchina, M. Z. Zgierski, and W. Siebrand, J. Chem. Phys. **109**, 1004 (1998).
[93]H. Ozeki, M. Takahashi, K. Okuyama, and K. Kimura, J. Chem. Phys. **99**, 56 (1993).
[94]J. H. Busch and J. R. De la Vega, J. Am. Chem. Soc. **108**, 3984 (1986).